Asian Journal of Chemistry; Vol. 25, No. 11 (2013), 5912-5916

ASIAN JOURNAL OF CHEMISTRY

http://dx.doi.org/10.14233/ajchem.2013.14165

Effect of WO_3 Addition Process on V_2O_5/TiO_2 Monolithic Catalysts

YUANYUAN HE*, QINGCAI LIU, JIAN YANG and WENCHANG XI

College of Materials Science and Engineering, Chongqing University, Chongqing 400044, P.R. China

*Corresponding author: Fax: +86 23 65111649; Tel: +86 13637951169; E-mail: heyuanyuan119@163.com

(*Received*: 6 June 2012; *Accepted*: 18 April 2013) AJC-13366

Selective catalytic reduction catalysts were prepared by introducing WO_3 with ammonium metatungstate instead of WO_3-TiO_2 powders. The surface and redox properties of these catalysts were investigated by BET, XRD, FT-Raman, H_2-TPR and catalytic activity test. The results showed that the catalyst prepared by new WO_3 addition technology had a less surface area and a smaller pore volume. However it exhibited a superior activity and presented a wider activity temperature window. The interaction of vanadia and tungsta on the surface of support was more intensify and consequently led to more octahedrally coordinated vanadyl species formed and tetrahedral wolframyl species appeared. These should be the reasons for the excellent performance of catalyst with WO_3 fed by ammonium metatungstate in mixed procedure.

Key Words: WO_3, Selective catalytic reduction, De-NO, FT-Raman spectroscopy, TPR.

INTRODUCTION

The selective catalytic reduction (SCR) of NOx by NH_3 is the most widely used technology for the control of NOx emission in flue gases from stationary sources due to its efficiency, selectivity and economy. Commercial de-NOx selective catalytic reduction catalysts in the form of monoliths or plates consist of V_2O_5 and WO_3 or MoO_3, which represent the active components and are supported on a high surface area of TiO_2 anatase carrier. Many studies[1-5] have shown that the promoter WO_3 inhibits the initial sintering of anatase TiO_2 and the transition of anatase to rutile, imparts to the catalyst strong Lewis and Bronsted acidity so as to enhance the NO removal activity of V_2O_5/TiO_2 catalyst. Besides, WO_3 is reported to not only widen the temperature window of selective catalytic reduction, increase the poison resistance to alkali metal oxides and arsenious oxide, but also reduce ammonia oxidation as well as SO_2 oxidation[1,4,6-9].

Previous investigations[4,6-13] focused on the influence of the loading of WO_3 on catalyst by preparation methods such as the impregnation with aqueous solutions of tungstate salts or grafting of tungsten alkoxides. However, there are few works expanded on the feeding method and source of WO_3 for honeycomb monolithic catalysts[9,12]. From the available literatures, the influences of sequential and simultaneous grafting of vanadia and tungsta on the final properties of the catalysts were investigated by Reiche *et al.*[14,15]. Furthermore, the relevant studies on the influence of different addition process of WO_3 in mixed pugging procedure on the V_2O_5/TiO_2 monolithic catalysts have not been reported. In this work, the structural, morphological, physicochemical characteristics of V_2O_5-WO_3/TiO_2 catalyst made by ammonium metatungstate addition process in mixed pugging procedure are reported. XRD, BET, FT-Raman, H_2-TPR and catalytic activity tests were employed with the purpose of clarifying the surface and redox properties of this catalyst. The results were compared to that of WO_3 in catalyst introduced by WO_3-TiO_2 powders (the traditional process).

EXPERIMENTAL

Catalyst preparation: Two addition process of WO_3 were employed in the present study (Fig. 1). Appropriate amounts of ammonium metavanadate (1.5 wt % V_2O_5 in catalyst) were dissolved in the solution of oxalic acid. The catalyst sample was prepared by extrusion molding with WO_3 introduced by precursor in Erich-kneader. An aqueous solution including an appropriate amount of ammonium metatungstate (5 wt% WO_3 in catalyst) was added to industrial anatase-TiO_2 powders in Erich-Kneader. Then they were mixed thoroughly and kneaded with the solution of ammonium metavanadate, a small amount of binding agent (fiber glass) with a suitable amount of distilled water. Whereafter, the resultant blend was molded with an extrusion molding device to produce a honeycomb monolith with an outer diameter of 75 mm × 75 mm, mesh of 6.2 mm and length of 450 mm. The obtained honeycomb monolith was dried and calcined subsequently and this sample was

denoted in the following as A. For comparison, the WO_3-TiO_2 powders (5 wt % WO_3 in catalyst) were directly placed into Erich-Kneader, also thoroughly mixed and kneaded with other materials as described above. The follow-up molding, drying and calcining processes were as the same as above and this sample obtained was denoted as B.

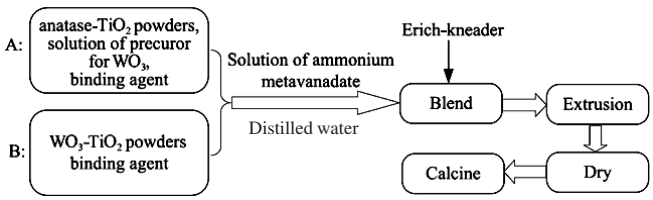

Fig. 1. Schematic of catalysts preparation

Catalyst characterization: Specific surface area and pore volume were determined from adsorption-desorption isotherms of N_2 at -196 ºC using a Micromeritics ASAP 2010 apparatus, after pretreating the samples for 2 h under vacuum at 300 ºC. XRD of the catalysts employed in the present study were examined by a Rigaku D/max-1200 X-ray diffractometer with Cu K_α radiation. The step scans were taken over the range of 2θ from 10º to 90º at scanning rate of 5º min^{-1}. The FT-Raman spectra of catalyst samples were recorded using a RFS-100 FT-Raman spectrometer with the 1064 nm line of a Nd:YAG laser as excitation source. The laser power was 50-150 mW and the spectral resolution was set to 4 cm^{-1}. The H_2-TPR measurements were carried out in continuous mode using a U-type quartz micro-reactor. A sample of about 100 mg was contacted with a H_2:N_2 mixture (5 % volume of H_2 in N_2) at a total flow rate of 30 mL min^{-1}. The sample was heated at a rate of 10 ºC min^{-1} from room temperature to 900 ºC. The hydrogen consumption was monitored using a thermal conductivity detector (TCD).

Catalytic activity measurements: Catalytic activity measurements in the de-NOx reaction were performed in a quartz tubular fixed-bed microreactor (i.d. = 14 mm), which inserted into an electric furnace and operated at atmospheric pressure. Volumes of 1.54 cm^3 (20-40 mesh) of catalyst granules were used for the test. The reaction gas mixture consisting of NH_3 (500 ppm), NO (500 ppm), O_2 (2 % by volume) with N_2 was used as the carrier gas and fed into the reactor with a total flow rate of 262 cm^3 min^{-1}, yield a gas hourly space velocity (GHSV) of 10,000 h^{-1}. Activity data were collected at different temperatures in the range of 200-500 ºC. The reaction system was held for 0.5 h at each reaction temperature until reached to a steady state before each test was performed. Analysis of NO concentration was carried out by using a KM9106 type gas analyzer. The definition of NO conversion is as follows:

$$\text{NO conversion} = \frac{NO_{in} - NO_{out}}{NO_{in}} \times 100$$

RESULTS AND DISCUSSION

Morphology and XRD: Table-1 summarizes results of BET surface area and XRD measurements for catalyst samples with different WO_3 addition methods. All specific surface areas

TABLE-1
MORPHOLOGICAL PROPERTIES OF CATALYSTS

Samples	S_{BET} (m^2 g^{-1})	V_{pore} (cm^3 g^{-1})	D_{pore} (nm)	Phase	D_{crist} (TiO_2 anatase) (nm)
A	53.46	0.2331	14.4	Anatase	21.50
B	59.70	0.2486	13.9	Anatase	20.24

of the tested samples are larger than 50 m^2 g^{-1}. The adsorption-desorption isotherms of nitrogen (Fig. 2) are type IV according to IUPAC classification and exhibit a H1 hysteresis loop, which are typical for mesoporous materials[16,17]. The pore size distributions (Fig. 3) are calculated from the desorption branches of the isotherms using the Barrett Joiner Halenda (BJH) method. The BET surface area of sample A is found to be significantly smaller while the pore volume is found to be slightly lower than sample B. This could be attribute to catalyst A shows narrower pore size distribution with a maximum pore diameter 17.21nm and a larger average pore diameter.

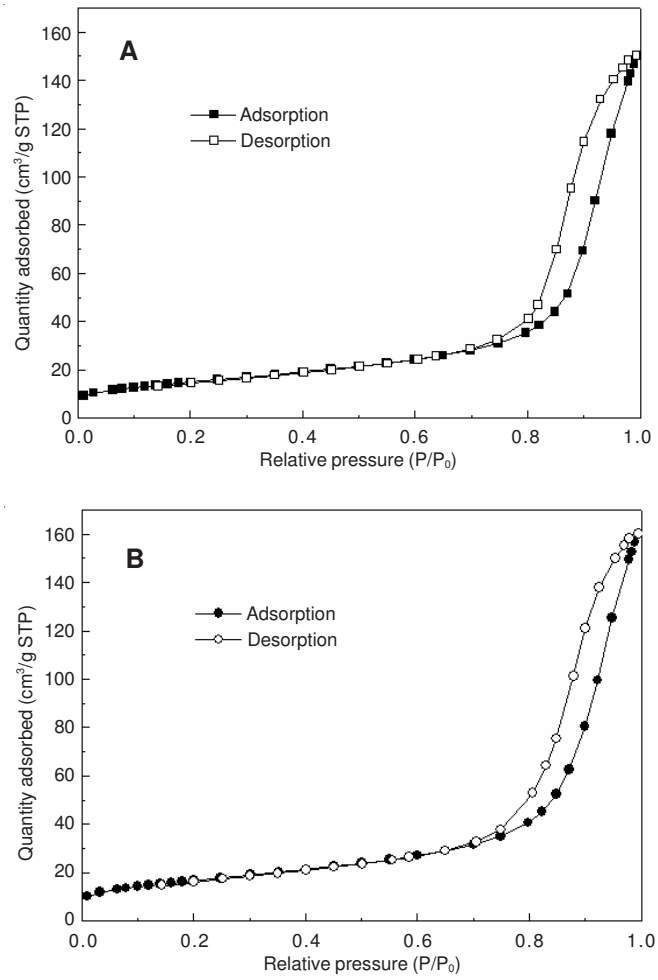

Fig. 2. N_2 adsorption-desorption isotherms

The XRD spectra of the samples are presented in Fig. 4. For both catalyst samples A and B, the anatase phase of TiO_2 is detected by XRD but the rutile phase is not seen, this means that no significant rutilization occurred under all applied preparation conditions. That no indication of crystalline V_2O_5 or WO_3 is found in the XRD spectra, indicated a high dispersion of both oxide species on the TiO_2 support. This characterization

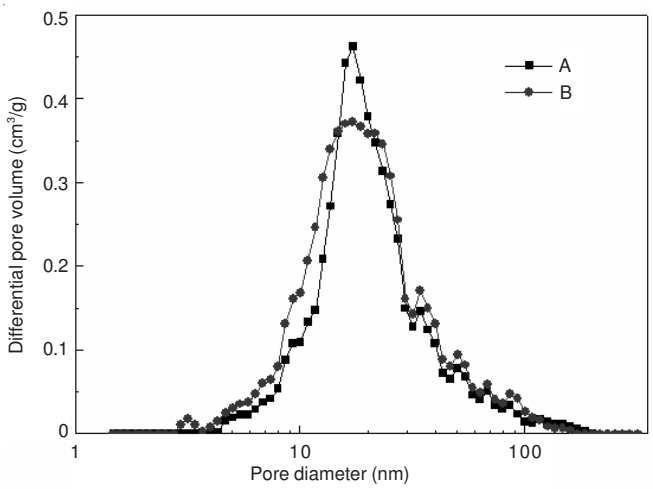

Fig. 3. Pore size distribution

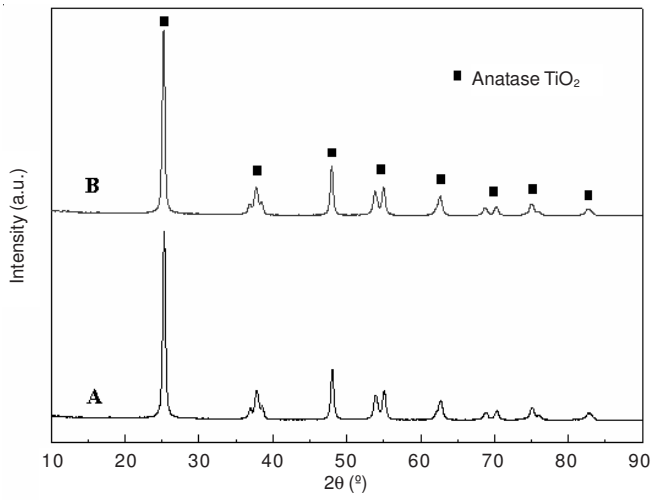

Fig. 4. XRD spectrum diagram

is in agreement with the previous literature[18], that in commercial selective catalytic reduction catalysts and the lower crystallinity or amorphous of catalyst structure is beneficial to NH_3-selective catalytic reduction reaction.

The crystallite size of anatase were estimated by Sherrer equation:

$$d = \frac{K\lambda}{\beta\cos\theta}$$

where K is a constant that depends on the shape of the particles and is generally assumed to be 0.89, λ is the wavelength of the X-ray radiation, β is the full width at half maximum (FWHM) of the considered diffraction peak and θ its position. The crystallite dimensions in line with results of BET are presented in Table-1, the smaller in the observed BET surface area of catalyst A, the larger in the mean pore radius and the reduction in the pore volume originated from crystallites growth and aggregate. This may be because W^{6+} ions and V^{5+} ions decomposed from ammonium ammonium metatungstate and ammonium ammonium metavanadate were reduced to corresponding low valence ions, afterwards attempt to entering TiO_2 crystalline lattice during the calcination process of catalyst A. And they promote aggregation of anatase, then larger pores are formed and a corres-pondent decrease in the surface area is measured[19].

FT-Raman: The surface structure of vanadium and tungsten on catalyst were examined by FT-Raman spectroscopy, as shown in Fig. 5. It has been generally acknowledged that the band around 1,030 cm^{-1} is associated with V=O bridge of monomeric vanadyl and the band around 900-1000 cm^{-1} with V-O-V bridge of polymeric vanadyl species[1,2,5,19-21]. The present result shows that no peak around 1,030 cm^{-1} appeared for two catalyst samples. However, distorted octahedrally coordinated VO_6 species[14] are recognized by a band at 988 and 979 cm^{-1} for catalyst A and B, respectively under ambient conditions. According to previous reports[1,3,14,15,18-21], specific activity of polymeric vanadyl species in selective catalytic reduction reaction is higher than that of monomeric vanadyl species. Furthermore, the peak of octahedrally coordinated vanadyl species for catalyst A is sharper than B, that is presumably caused by the reason that the interaction of vanadia and tungsta on the surface of support is more intensity with WO_3 fed by ammonium metatungstate in mixed procedure. The band around 800 cm^{-1} consists of the overlapping contribution of a second-order anatase feature and of the W-O-W stretching of octahedrally coordinated W units in an environment similar to the one of bulk WO_3[19,20,22]. It is worth noticing that the weak peak around 1050 cm^{-1} indicates a small fraction of tetrahedrally coordinated tungsten oxide is present in catalyst A. According to Gutiérrez-Alejandre *et al.*[23,24], these surface tetrahedral wolframyl species were coordinatively unsaturated and acted as strong Lewis acid sites, which is beneficial to the exerting of catalytic activity.

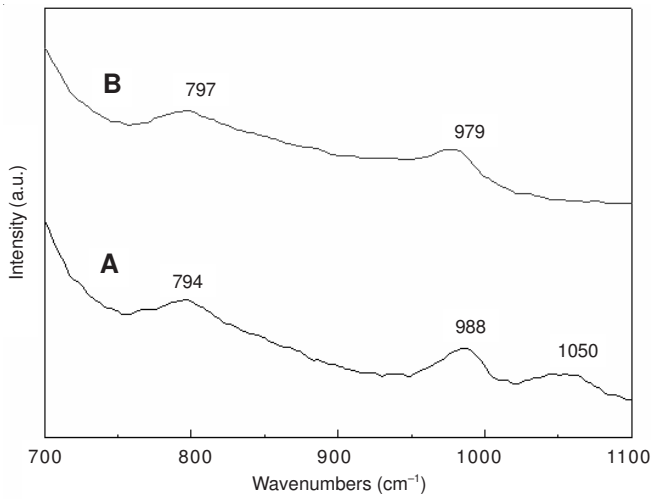

Fig. 5. Raman spectrum diagram of catalysts

There is no evidence for the presence of crystalline vanadia or tungsta found by XRD or by more sensitive Raman technique, which indicates that V_2O_5, WO_3 are well dispersed on the surface of the support. The structure of vanadium is slightly influenced by the different addition method of WO_3, while tetrahedral wolframyl species is found with WO_3 of catalyst A introduced by ammonium metatungstate in mixing procedure.

H_2-TPR: TPR experiment of H_2 were performed over the catalyst A and B in order to clarify the influence of WO_3 addition process on dispersion of active species in V_2O_5/TiO_2 monolithic catalysts. Although the reduction profiles of both catalysts are somewhat different from each other (Fig. 6), each

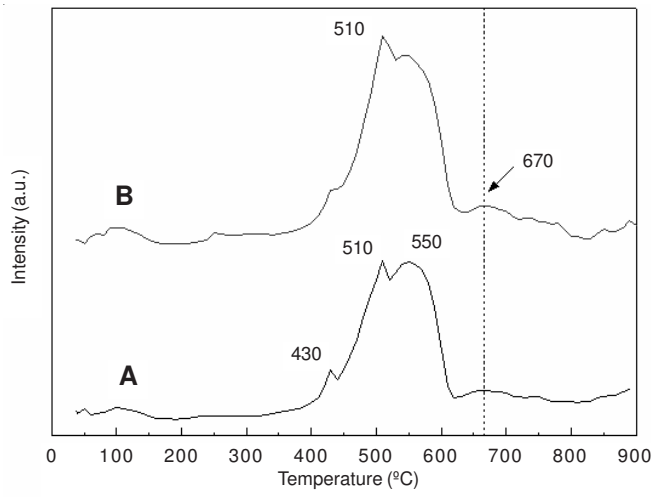

Fig. 6. H_2-TPR profiles of catalysts

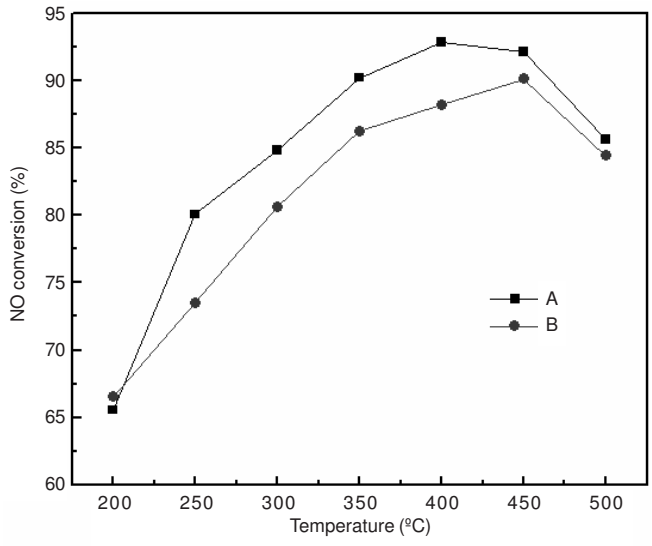

Fig. 7. Comparison of catalytic activities

profile seems to be of one major reduction peak the temperature range from 450 to 600 ºC. This peak corresponds to the hydrogen consumption by the reduction of V^{5+} to V^{3+} in agreement with previous literature reports[6,21,25,26]. The bigger peak area, the greater its hydrogen absorbing, which is beneficial to the selective catalytic reduction reaction. Meanwhile, weak peaks emerge at about 670 ºC on TPR profile for catalysts are attribute to the reduction[6,14,15] of W^{6+} to W^0. TPR peaks around 510 and 670 ºC of sample A are weaker comparing with B, this may be the result of the W^{6+} ions and V^{5+} ions decomposed from ammonium metatungstate and ammonium metavanadate were reduced to corresponding low valence ions. All samples showed the presence of a reduction peak of minor intensity at 430 ºC attributed to the reduction of vanadium highly dispersed and strongly interacted with the support. As this peak is visible stronger and it agrees well with the result of Raman that the band is assigned to octahedrally coordinated VO_6 species is shaper than catalyst B. It can be concluded that catalyst A presents a higher dispersion of vanadium oxide species on the support.

Activity test for NO reduction by NH_3: Fig. 7 shows the NO conversion at various temperatures for selective catalytic reduction of NO by NH_3 over catalyst samples. Similar results are obtained in the case of catalysts with different feeding method of WO_3, the NO conversion are enhanced with elevating reaction temperature among 200-400 ºC. It can be seen that, the maximum activity measured over catalyst A is 93 % at 400 ºC, but declines around 450 ºC because of secondary products NOx generated by the oxidation[1] of NH_3. While the NO conversion of catalyst B reaches a peak nearly at 500 ºC, also falls sharply subsequently due to similar reactions as describe above. Consequently, catalyst A exhibits a superior selective catalytic reduction activity compared to the sample B in a wider temperature region from 250 to 500 ºC, although the catalyst B developed in this work has a higher specific surface area of 59.70 $m^2\ g^{-1}$ and a larger porous volume of 0.2494 $cm^3\ g^{-1}$. It can be hypothesized that decreasing in the catalyst surface area favours the aggregation of isolated vanadyl to form polymeric species. Polymeric vanadyl species likely present a greater mobility of lattice oxygen[27] and thus, a higher reducibility, as indeed observed experimentally by Raman in this work.

Conclusion

The catalyst B made by WO_3-TiO_2 powders addition process in mixed procedure was found to possess a higher surface area and a larger porous volume. No crystalline vanadia or tungsta formed indicated a high dispersion of both oxide species on the TiO_2 support though WO_3 fed by different process. Polymeric vanadyl species was the main structure of vanadium for both catalysts in favour of specific activity in selective catalytic reduction reaction. There were no significant differences between the catalyst A and B. The interaction of vanadia and tungsta on the surface of support was more intensity with WO_3 fed by ammonium metatungstate in mixed procedure, which led to more octahedrally coordinated vanadyl species formed and tetrahedral wolframyl species appeared. Thus, catalyst A presented a superior activity and has a wider active temperature window.

ACKNOWLEDGEMENTS

The authors are grateful for the financial support of the National High-Tech Research and Development(863) Program of China (No.2010AA065001), Sci-Tech Personnel Service for Enterprise (No. 2009GJF10047) and National Natural Science Fund of China (No. 51274263 and No. 51204220).

REFERENCES

1. L.J. Alemany, L. Lietti, N. Ferlazzo, P. Forzatti, G. Busca, E. Giamello and F. Bregani, *J. Catal.*, **155**, 117 (1995).
2. L.J. Alemany, F. Berti, G. Busca, G. Ramis, D. Robba, G.P. Toledo and M. Trombetta, *Appl. Catal. B*, **10**, 299 (1996).
3. M.D. Amiridis, R.V. Duevel and I.E. Wachs, *Appl. Catal. B*, **20**, 111 (1999).
4. A. Scholz, B. Schnyder and A. Wokaun, *J. Mol. Catal. A*, **138**, 249 (1999).
5. P. Forzatti, *Appl. Catal. A*, **222**, 221 (2001).
6. S.T. Choo, S.D. Yim, I.-S. Nam, S.-W. Ham and J.-B. Lee, *Appl. Catal. B*, **44**, 237 (2003).
7. S. Djerad, L. Tifouti, M. Crocoll and W. Weisweiler, *J. Mol. Catal. A*, **208**, 257 (2004).
8. J.W. Choung, I.-S. Nam and S.-W. Ham, *Catal. Today*, **111**, 242 (2006).
9. M. Kobayashi and K. Miyoshi, *Appl. Catal. B*, **72**, 253 (2007).
10. J. Engweiler, J. Harf and A. Baiker, *J. Catal.*, **159**, 259 (1996).
11. S. Eibl, B.C. Gates and H. Knozinger, *Langmuir*, **17**, 107 (2001).
12. M. Kobayashi and M. Hagi, *Appl. Catal. B*, **63**, 104 (2006).

13. X. Zhang, X. Li, J. Wu, R. Yang and Z. Zhang, *Catal. Lett.*, **130**, 235 (2009).
14. M.A. Reiche, T. Burgi, A. Baiker, A. Scholz, B. Schnyder and A. Wokaun, *Appl. Catal. A*, **198**, 155 (2000).
15. M.A. Reiche, P. Hug and A. Baiker, *J. Catal.*, **192**, 400 (2000).
16. L.C.Y. Segura, P. Kustrowski, P. Cool, R. Dziembaj and E.F. Vansant, *J. Phys. Chem. B*, **110**, 948 (2006).
17. A.L. Ahmad, C.P. Leo and S.R.A. Shukor, *J. Porous Mater.*, **16**, 33 (2007).
18. L. Baraket, A. Ghorbel and P. Grange, *Appl. Catal. B*, **72**, 37 (2007).
19. I. Nova, L.D. Acqua, L. Lietti, E. Giamello and P. Forzatti, *Appl. Catal. B*, **35**, 31 (2001).
20. G. Madia, M. Elsener, M. Koebel, F. Raimondi and A. Wokaun, *Appl. Catal. B*, **39**, 181 (2002).
21. I. Giakoumelou, C. Fountzoula, C. Kordulis and S. Boghosian, *J. Catal.*, **239**, 1 (2006).
22. K.K. Akurati, A. Vital, J.P. Dellemann, K. Michalow, T. Graule, D. Fetti and A. Baiker, *Appl. Catal. B*, **79**, 53 (2008).
23. A. Gutierrez-Alejandre, J. Ramirez and G. Busca, *Langmuir*, **14**, 630 (1998).
24. A. Gutierrez-Alejandre, P. Castillo, J. Ramirez, G. Ramis and G. Busca, *Appl. Catal. A*, **216**, 181 (2001).
25. S. Albonetti, S. Blasioli, A. Bruno, J.E. Mengou and F. Trifirò, *Appl. Catal. B*, **64**, 1 (2006).
26. H. Guo, D. Li, D. Jiang, H. Xiao, W. Li and Y. Sun, *Catal. Today*, **158**, 439 (2010).
27. S. Djerad, M. Crocoll, S. Kureti, L. Tifouti and W. Weisweiler, *Catal. Today*, **113**, 208 (2006).